LUND UNIVERSITY
Faculty of Science

Formation of cobalt oxide clusters on oxygen modified graphene

Robin Schneider

Thesis submitted for the degree of Bachelor of Science
Project duration: 04 months

Supervised by Jan Knudsen

Department of Physics
Division of Synchrotron Radiation Research
May 2015

Abstract
Aim of this thesis is to study and characterize the formation of cobalt oxide clusters on graphene. The performed experiments consist of three different steps. First, a monolayer graphene film is grown with temperature programmed growth and chemical vapor deposition on an Iridium (111) single crystal surface. Second, the graphene film is exposed to oxygen radicals, which bind to the film and form clusters. In the last step, cobalt oxide was deposited onto the O-functionalized graphene film to form cobalt oxide clusters atop the oxygen clusters.
The evolution of the experiment is studied with x-ray photoelectron spectroscopy. The recorded data of the C 1s spectrum from the O-functionalization experiment are coherent with recently published literature on the same topic. The Ir $4f_{7/2}$ suggests that 6.5% of the carbon atoms are bound in an epoxy group. Furthermore the Ir $4f_{7/2}$ spectra show exclude intercalataion of oxygen or cobalt oxide. Subsequent deposition of cobalt oxide on the O-functionalized graphene film leads to cobalt oxide in rocksalt structure containing Co^{2+} ions. The ratio of cobalt oxide and the epoxy group is 1:1 which suggest the formation of cobalt oxide cluster onto the oxygen radicals. Nonetheless, further scanning tunneling microscopy experiments have to be performed to describe the stability, structure, size and coverage of these clusters. This is briefly discussed in the outlook.

Contents

Acronyms

fcc	face centered cubic
TPG	Temperature Programmed Growth
CVD	Chemical Vapor Deposition
STM	Scanning Tunneling Microscopy
LEED	Low Energy Electron Diffraction
XPS	X-ray Photoelectron Spectroscopy
CLS	Core Level shift

1 Introduction

Many things in our modern society were not possible without the use of catalysts. For example, they efficiently convert toxic gases(e.g. CO and NO) produced in the car engine to less toxic gases (CO_2 and N_2). Another important catalytic reaction is the Haber-Bosch-process. In this process nitrogen (N_2) and hydrogen (H_2) react with each other with the help of a metallic catalyst at a high temperature and pressure and ammonia (NH_3) is formed. This process is essential for the production of ammonia in a large scale which is used nowadays for the production of fertilizer.
Catalysts make a thermodynamically possible chemical reaction run faster. Some chemical reactions do not occur without the help on a catalyst even though the Gibbs free energy of the product molecules are lower than the energy of the reactants; i.e. the reaction is thermodynamically possible. Without the catalyst a high activation energy of the gas phase or liquid phase reaction is blocking the reaction. In contrast the catalyzed reaction takes place on the catalysts surface, which lowers the activation energy significantly. Taking for example a chemical reaction like: $A + B \rightarrow AB$. The atoms A and B separately adsorb onto the surface, react with each other and finally desorb as a AB molecule.
Most of the catalysts we know today have been found by trial and error. This is neither a cost nor time efficient method. Thereby, surface science is focused on a better understanding of catalytic processes in order to develop more efficient catalysts in the future. A lot of research is done in the area of artificial photosynthesis. Part of the photosynthesis is the cracking of water into hydrogen and oxygen:

$$2H_2O \longrightarrow 4H^+ + 4e^- + O_2 \tag{1}$$

With hydrogen, which can be used as fuel, and oxygen as products this is a very important reaction. Furthermore, water has no production costs and is everywhere available on earth. However, without a catalyst the reaction occurs only at temperatures of 2500 °C and higher[1]. Existing catalysts for this reaction are made of rare and expensive metals[2]. Therefore, it is favorable to develop new catalysts based on cheaper materials. In 2009 Jiao *et al.* published a paper about cobalt oxide clusters supported by mesoporous silica and showed that this material is an efficient oxygen evolving catalysts under mild temperatures and pH conditions [3]. In their study the cobalt oxide had a spinel structure (Co_3O_4). Following their ideas one could search for alternative ways to form well ordered cobalt clusters to get a detailed understanding of H_2 adsorbtion on cobalt oxide. Recently, it has been demonstrated that exceptionally well ordered metal clusters can be grown on graphene. Thereby, I will use graphene as a support material to grow and characterize cobalt oxide clusters.

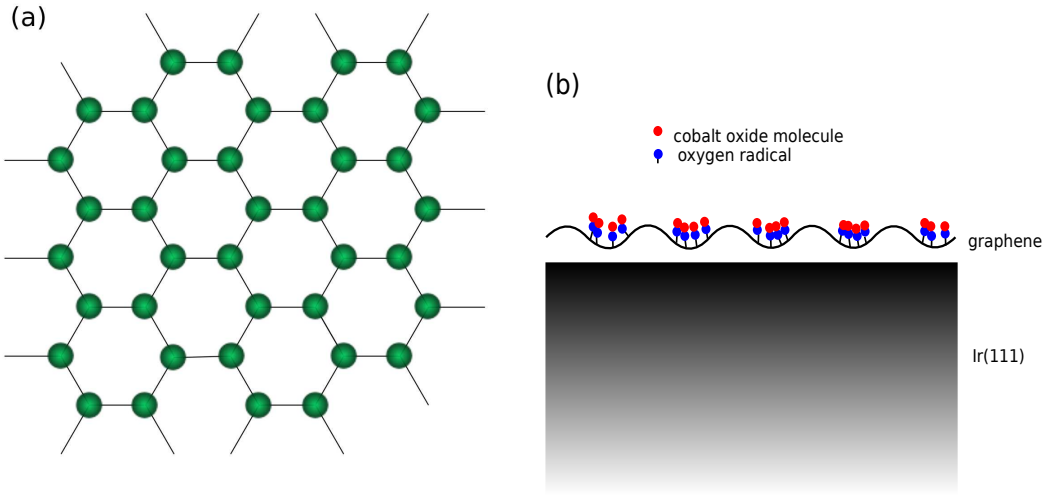

Figure 1: Panel (a) shows the atomic structure of a single layer of graphite, which is also known as graphene. In panel (b) is a schematic illustration of the experiment this thesis will focus on.

Graphite is well studied and its atomic structure has been known for decades. In summary, graphite consists of carbon layers bound to each other by weak van der Waals bindings. Within each layer the carbon atoms form a two dimensional hexagonal lattice with sp^2 hybridized carbon atoms. Three of the four valence electrons are located in the sp^2 orbitals, while the last electron is located in a delocalized π orbital. The atomic structure of a single layer of graphite is shown in figure 1.
Graphene is a new material that was recently isolated from graphite by Andre Geim and Konstantin Novoselov in 2004[4], although it was already predicted in 1984[5]. In their work, Geim and Novoselov managed to isolate and characterize a single atomic carbon layer from graphite and this is what we today name graphene. The atomic structure of graphene is very similar to graphite, with sp^2 hybridized C-atoms and a delocalized π network, but the pure 2D architecture of the material leads to many spectacular properties:
Graphene is a zerogap semiconductor, also called a semi-metal. The electron mobility is 15,000 $\frac{\mathrm{cm}^2}{\mathrm{Vs}}$[6]. This is very high especially compared to materials that are used in electronic devices such as copper (0.32 $\frac{\mathrm{cm}^2}{\mathrm{Vs}}$) and silicon (1,600 $\frac{\mathrm{cm}^2}{\mathrm{Vs}}$)[7].
Besides the spectacular electronic properties, graphene also has some remarkable mechanical properties. With a tensile strength of 130,000 MPa [8] it is stronger than most known materials. For example, steel commonly has a strength of $\approx$ 500 MPa , which is only about 0.004% of graphene. The Young modulus of graphene is 1,050 GPa [9]. Only diamond has a higher Young modulus. With these electronic and mechanical properties graphene has a large potential as a new and improved material, both for electronic devices and in mechanic constructions. Especially if one takes into account that the raw

material of graphene, carbon, is cheap as there are plenty of carbon resources on earth. With this in mind and to facilitate a rapid implementation of graphene in new products, the European Union decided to support the research in graphene with 1 billion Euros in 2013[10].
However, our interest in graphene is not due to the spectacular electronic or mechanical properties. Rather, it originates from the fact that graphene can also be used as a support material for metal and oxide clusters. Graphene grown on a metal substrate forms a moiré pattern with a nano mesh surface, which has a modulated height variation leading to hills and valleys. The height variation makes the deposition of atoms in certain regions possible and thereby the creation of well ordered structures. The nano mesh ranges over a size of several μm and is therefore extraordinary well suited for the analysis and study of basic catalytic processes. Vinogradov *et al.* recently studied the deposition of atomic oxygen onto graphene. For low coverages oxygen radicals prefer to adsorb in certain regions of the moiré pattern; hence, it is possible to form oxygen clusters on graphene. Using these oxygen clusters as seeds for the growth of cobalt oxide could potentially lead to the formation of well ordered cobalt oxide clusters (see figure 1 (b) for a sketch). The goal of this thesis is to study if it is possible to form these well ordered cobald oxide cluster and characterize their structure.

2 Background

2.1 Structure of graphene on Ir(111)

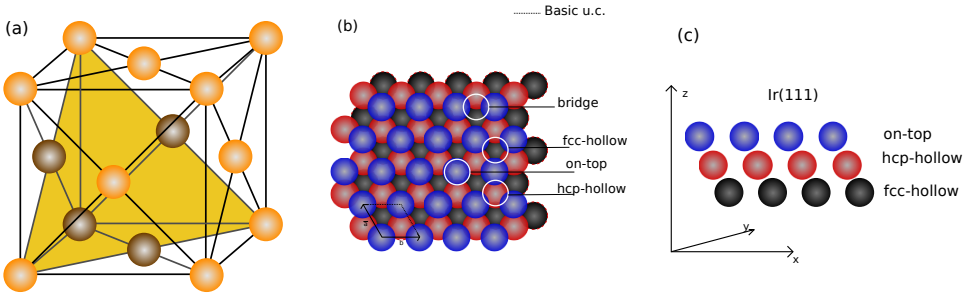

Figure 2: Panel (a) shows the (111) plane in an fcc unit cell, panel (b) the Ir(111) plane in perpendicular view and panel (c) a side view.

2.1.1 Structure of Iridium

Iridium has a face centered cubic (fcc) crystal structure as shown in figure 2(a). The (111) plane has a hexagonal unit cell with a lattice constant of 2.71 Å[11]. Panel (b) shows an on top view of Ir(111). Within the unit cell four different sides, on-top, bridge,

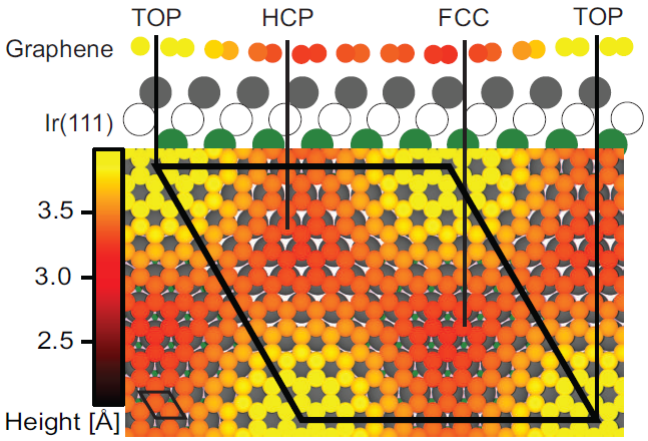

Figure 3: Ball model of graphene/Ir(111) adapted from Elin Grånaes [12].

hcp-hollow and fcc-hollow, can be identified. Panel (c) shows a sideview of the Ir(111) structure.

2.1.2 Graphene on top of Ir(111)

Graphene (Gr) has a honeycomb structure with a neighbour neighbour atomic distance between two carbon atoms of 1.42 Å[13]. The lattice constant is 2.46 Å and hence slightly smaller than the one of Ir(111) see figure 3 [14]. This mismatch in lattice constants of graphene and Ir(111) is responsible for the formation of a so called moiré pattern, which repeats itself over the whole surface every 25.3 Å[15]. Consider a carbon ring in a TOP domain, with an on-top Ir(111) atom bellow its center. A few unit cells away there will no longer be a on-Top atom bellow its center. Instead the rings will have hcp-hollow or fcc-hollow sites in their center due to the lattice mismatch. These regions are, therefore, called HCP and FCC domains, respectively. Since the carbon carbon atoms in the HCP/FCC domains are located on top of Ir(111) surface atoms, they are bend more strongly towards the Ir(111) as a results of an mixing of the carbon π and iridium $d_{3z^2-r^2}$ orbitals [16]. This follows a lower graphene-Ir(111) distance and as a consequence a hilly graphene landscape. After several more unit cells there will be a TOP domain again and the pattern repeats itself, see figure 3. There are 200 carbon atoms and 87 $\pm$ 3 iridium atoms in each moiré unit cell [15].

2.2 Graphene growth

There are different methods of graphene production. First, the mechanical method called cleavage. Here, one uses e.g. adhesive tape to remove single layers of graphene from a sample of graphite. A second method is to use graphite oxide. As graphite oxide is hydrophilic, it breaks in water to macroscopic flakes which are mostly one layer thick. With subsequent partial reduction one can now get graphene out of these flakes.

The graphene used for my experiment is produced by two different methods: temperature programmed growth (TPG) and chemical vapor deposition (CVD). Both methods are based on the same concept of cracking a hydrocarbon gas on a metallic surface. For my experiments I used an Ir(111) single crystal surface as the substrate. Ir(111) has the advantage, compared to other metals like platinum, that it is possible to form large areas of graphene over several μm with the same orientation on the surface [17].

2.2.1 Temperature programmed growth

The basic principle of TPG is to expose the metal substrate at room temperature to the hydrocarbon gas followed by annealing the sample. The hydrocarbon molecules, in our case C_2H_4, first adsorb on the Ir(111) surface and saturates it. Upon heating C_2H_4 dissociates and the carbon atoms stick and form graphene while the hydrogen forms H_2 that desorbs into the vacuum. Temperatures of at least 820K are needed to release the hydrogen [18]. I used, however, 1100K in my experiment to obtain well ordered graphene.
With a dose of 2.7 L ($2 \cdot 10^{-8}$mbar for 30s) of C_2H_4 the Ir(111) surface is saturated. Subsequent annealing to 1100K dissociates the C_2H_4 molecules and leaves 20% of the Ir(111) surface covered by graphene islands [19]. Therefore, every cycle covers the surface with additional 20% of the uncovered area. Hence, it is hard to grow a full monolayer with this method. The orientation of the islands is parallel to the substrate [12].

2.2.2 Chemical vapor deposition

In order to get a full monolayer of graphene the CVD method is used, which in many ways is similar to the TPG method. The only difference between the two methods is the exposing temperature. In CVD growth exposure is done at a high temperature, which plays an important role for the rotation of the graphene. Possible rotations are R0°, R14°, R18.5° and R30° [20; 21] using a temperature of 1000K, which gives a full layer of graphene mixed with different rotations. However, the only possible monolayer with only one rotation is R0° which can be achieved with a temperature of 1320K [12]. Temperatures of this order have the disadvantage that not only the hydrogen atoms dissociate from the substrate, but also some carbon atoms. Furthermore it is often difficult to achieve that high temperature in the setup. Therefore one often combines CVD and TPG [20]. Beginning with a cycle of TPG first to get the correct orientation and a cycle of CVD afterwards to create a full monolayer graphene film.

3 Experimental procedure

I used three different techniques in my studies: Scanning Tunneling Microscopy (STM), High Resolution X-ray Photoelectron Microscopy (HRXPS), and Low Energy Electron Diffraction (LEED).

3.1 Low Energy Electron Diffraction

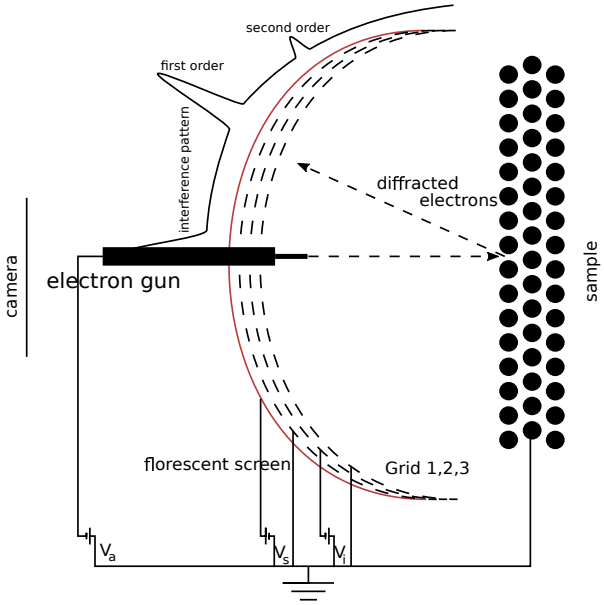

Figure 4: Sketch of a common LEED setup, consisting of an electron gun a fluorescent screen, a camera and three grids with different applied potentials $V_{i,a,s}$.

Low Energy Electron Diffraction (LEED) is a technique used to determine the surface periodicity of a sample. A schematic setup is presented in figure 4. Electrons are accelerated by an electric potential V_a towards the sample and become diffracted at the surface lattice. They interfere constructively with each other and are detected at a florescent screen. Before reaching the screen they pass three grids with different potentials. The first grid shields the potentials of the other grids and creates a field free region between the sample and the first grid. No electrostatic force acts therefore on the electrons in this region. A potential V_i is applied between grid 1 and 2 to block all inelastic scattered electrons and the potential V_s, between grid 3 and the screen, is used to accelerate the electrons towards the screen so that they have a high enough energy to create a florescence spot at the screen. The bright spots on the screen are then captured by a camera. The energy of the electrons is normally between $10-100$ eV. This corresponds to a wave length in the order of several Å according to de Broglie:

$$\lambda = \frac{h}{\sqrt{2mE}} \tag{2}$$

Lattice constants of surfaces are of similar size and an interference pattern is, hence, created by elastic scattered electrons. Since electrons have a high cross section with atoms and thus a low mean free path in matter they are mostly scattered by the surface and the first sublayers. The diffraction pattern on the screen corresponds to the reciprocal lattice of the sample, since the waves only interfere constructively in the case of:

$$R \cdot K = 2\pi \cdot n \tag{3}$$

With n being an integer, responsible for the order of the maximum, R the position vector of the surface plane, and K the difference in wave vector between the incident and the scattered wave. The reciprocal lattice can be described by the vector set G. G and R are connected by the following condition:

$$e^{iG \cdot R} = 1 \tag{4}$$

As a result of this the ratio of vectors in the real lattice is proportional to the inverse ratio of their reciprocal vectors which is often used to analyze LEED images and determine the lattice constants of the sample.
Two LEED images are shown in figure 5, the first is acquired on clean Ir(111) and the second one on 1ML graphene on Ir(111). Red arrows show the unit cells of the reciprocal lattice. With the help of the reciprocal vector length one can calculate the lattice constants of graphene and the moiré pattern. To minimize the error-bars, I will use the doubled length of the reciprocal vectors (see panel (b) diagonal red and blue arrows). The relationship

$$R * G = 2\pi \tag{5}$$

holds for all vectors and constants between reciprocal and real space. Therefore I only have to calculate the ratios of the inverse lengths to determine the real lattice constant. For iridium and graphene the ratio is 1.116 to 1, which results in a lattice constant of 2.43 Å. A similar calculation results in a lattice constant of 24.95 Å for the moiré pattern, slightly lower than the literature value.

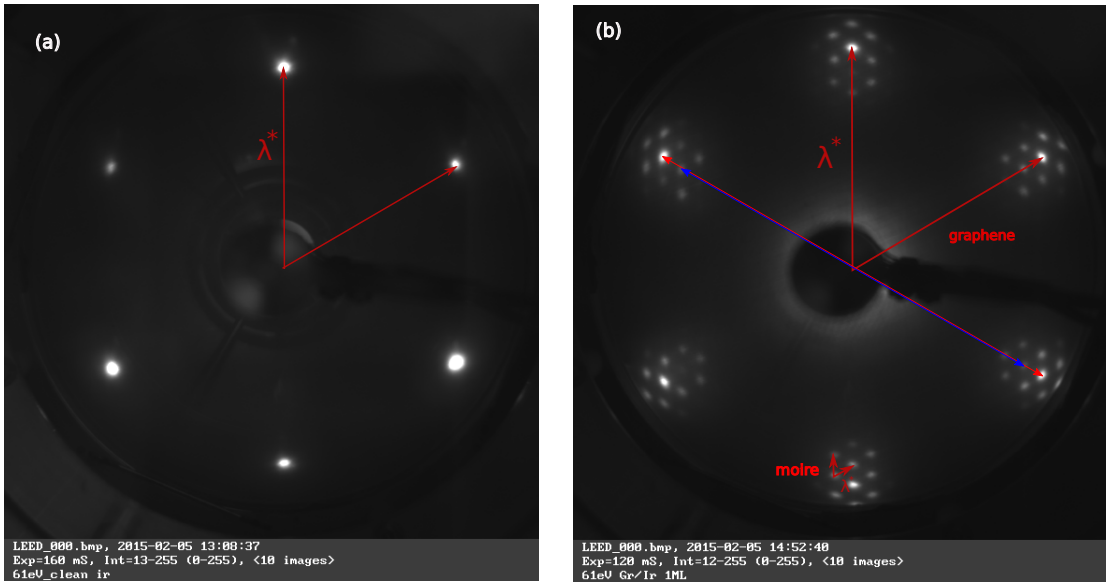

Figure 5: Left LEED image of clean Ir(111). Right LEED image of 1Ml Gr/Ir(111). The red arrows show the reciprocal unit cells of Ir(111) in (a), graphene and the moiré pattern in (b). Lambda is the reciprocal lattice constant.

3.2 Scanning Tunneling Microscopy

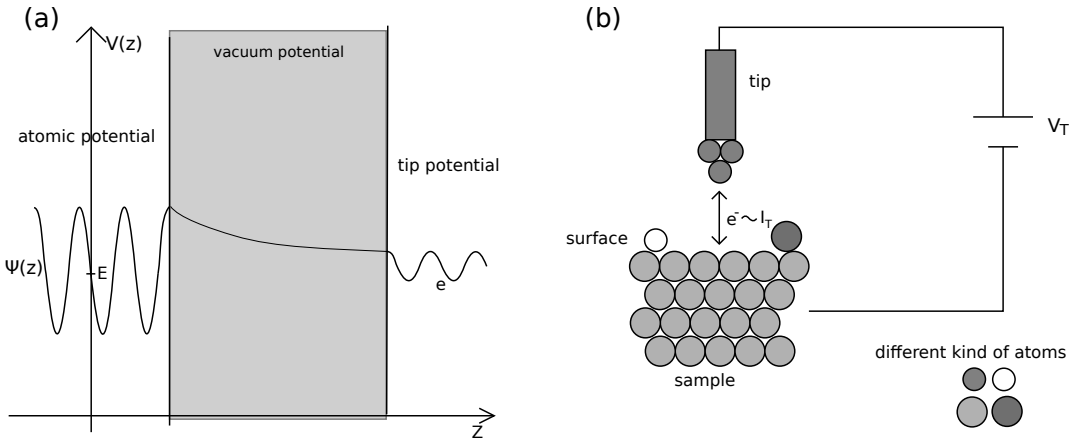

Figure 6: Quantum mechanical sketch of the tunneling effect with the electron wave function Ψ in panel (a). Panel (b) shows a schematica illustration of the STM setup.

In contrast to LEED Scanning Tunneling Microscopy (STM) is a real space surface sensitive technique. The Scanning tunneling microscope is able to give an image of the sample with atomic resolution. The technique was developed in 1981 by Gerd Binnig and Heinrich Rohrer and and they were awarded the Nobel Prize in Physics for their invention in 1986 [22; 23].
The basic concept of a STM is that a metal tip is raster-scanned above the sample surface. During the process the tip does not touch the sample. Instead it measures the current flowing between the tip and the sample. The current occurs due to a potential difference (0.01-3 V) applied between the sample and tip causing electrons to tunnel through the vacuum barrier between them. The measured current is proportional to the number of electrons that tunnel through the vacuum barrier, which depends exponentially on the tip-sample distance. It can be shown that the tunnel current (I) can be written as:

$$I(z) = VC \cdot \mathrm{e}^{-kz} \tag{6}$$

where C is a constant, which depends on the tip and sample material, V is the bias between them, and z the tip-sample distance. The exponential dependence on z can be explained by quantum mechanics. Consider the vacuum between the tip and the surface atom as an finite potential for the electron wave function (figure 6(a)). Classically the electron can not pass this barrier, but quantum mechanics dictates that the wave can tunnel into the barrier with an exponential decreasing amplitude. If the wave passes the vacuum, it starts oscillating again. As the square of the wave function is proportional to the probability to observe the electron, it is obvious that the current decreases for a larger distance between sample and tip. One should remember at this point that a higher current does not automatically imply a closer distance to the sample. An impurity or just a different atom on top of the surface can have a different density of states, which would result in a change of current, so the current could decrease although the atom is actually closer. Hence, we can only make a reliable prediction about the height of the surface for a clean sample.
An illustration of a typical STM setup is presented in figure 6(b). The resolution of STM depends on the radius of curvature of the tip. In an ideal scenario the tip consist of one single protruding atom. With such a tip it is possible achieve a resolution in height of better than 1 Å and in the plane perpendicular to the tip of 0.1 Å[24]. The setup can be operated in two different modes, with a constant current or with a constant height.
In constant current mode the tip-sample current is kept constant, meanwhile, the height is adjusted continuously with a feedback mechanism during the raster-scan above the surface. One advantage of this mode is that the tip is protected against large height difference within the surface, which could break the tip. In contrast to this mode the fixed height scan allows faster scanning but has the disadvantage that the tip easily crashes into the sample if it contains large height variations. I will use the constant current mode in my experiment.
STM measurements are heavily influenced by vibrations. Therefore, the STM equipment must be isolated against vibrations of the environment. This is normally achieved by suspending the STM stage by springs or using air legs.
Figure 7 shows overview (b) and atomically (a) resolved STM images of Gr/Ir(111).

With the only difference between HCP and FCC domains beeing in the second and third layer of Ir(111) these regions are expected to look very similar. Therefore, the bright regions in the STM images most likely correspond to the HCP and FCC domains, while the dark areas are the TOP domains. The measured height of the TOP domains, which is lower than in the HCP and FCC regions, is thus very different from the real height. This is in contrast to the model as they should have according to it the largest height above the Ir(111) substrate.

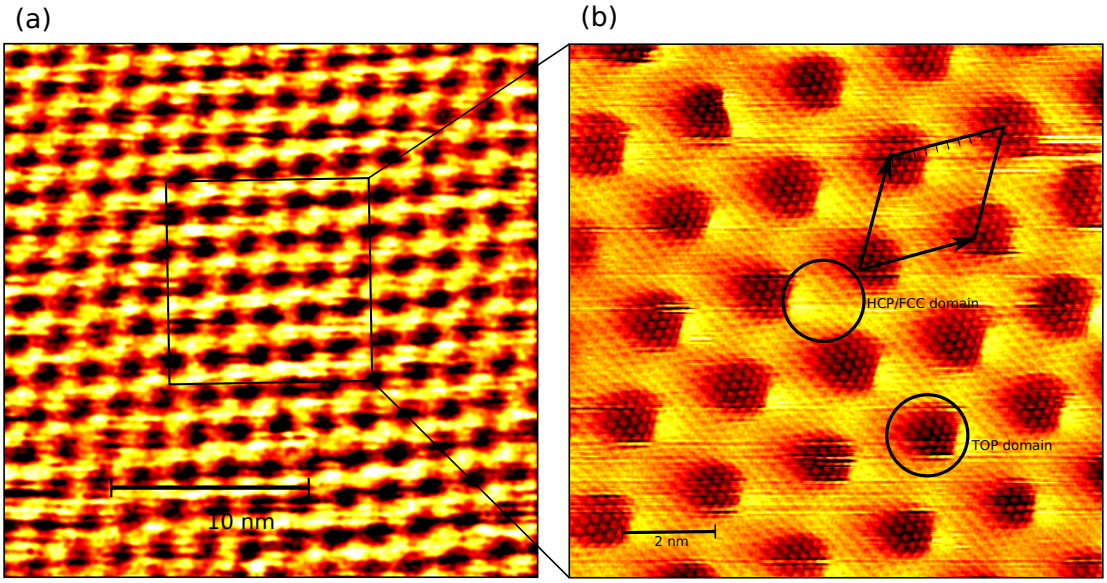

Figure 7: Two images of Gr/Ir(111).(a) 27x27 nm (b) 11x11 nm. Image (a) was recorded at a current of 60 pA and a voltage of 350 mV, image (b) at a current of 5 nA and a voltage of 20 mV.

3.3 X-ray Photoelectron Spectroscopy

3.3.1 Photoelectric effect

X-ray photon spectroscopy (XPS) is another surface sensitive technique used to analyze the surface and top layers of a sample. Based on the photoelectric effect it utilizes photoelectrons to determine the atomic elements of the sample and their chemical structure. The photoelectric effect was explained by A. Einstein in 1905. Einstein based his theory on a experiment performed by H. Hertz in 1887 [25; 26]. Einstein was in 1921 awarded the Nobel Prize in Physics for his theory since it introduced the idea of quantized light for the first time[27]. The photoelectric effect states that a photon can be absorbed by an atom if it has an energy above a certain threshold. The threshold energy is the binding energy between the electron and its atom. After absorption an electron leaves

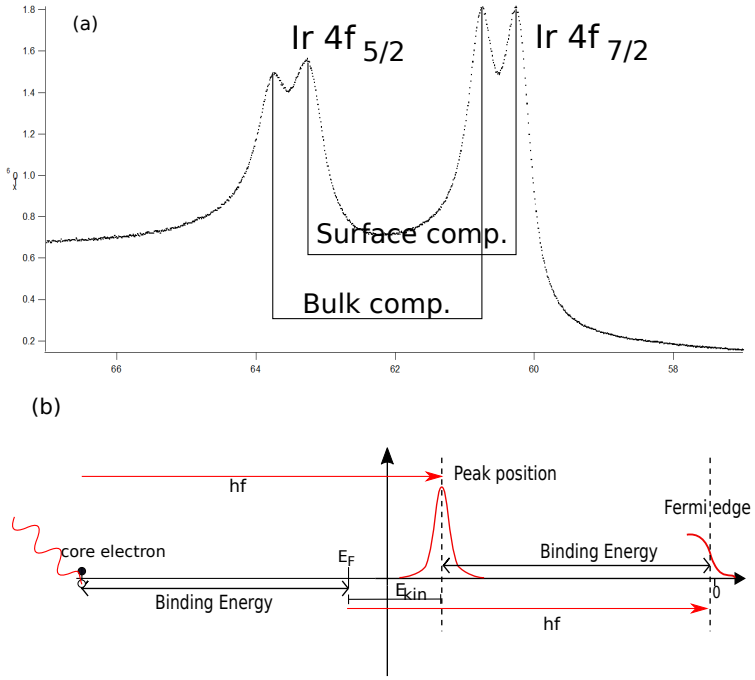

Figure 8: Panel (a) shows an uncalibrated Ir 4f spectrum recorded by a photon energy of 120 eV. In (b) is a schematic illustration of the photoemission process including the calibration of the system with help of the Fermi Edge.

the atom with a kinetic energy E_{kin}:

$$E_{photon} = h \cdot f = E_{bind} + E_{kin} \tag{7}$$

Due to the high cross section between electrons and matter, they are likely to scatter inelastically and lose kinetic energy. From this follows that XPS is a surface sensitive technique. Monochromatic light with a constant energy is then used to record a XPS spectrum. The number of electron as function of their kinetic energy is then measured for a small energy interval. Electrons ionized from core level will show up as a peak in the spectrum.
Figure 8 (a) shows a spectra of a pristine graphene film on Ir(111) recorded by a photon energy of 120 eV. The x-axis shows the binding energy of the electrons, calculated from the kinetic energy and the photon energy ($E_{bind} = h \cdot f - E_{kin}$), since an increasing kinetic energy results in a smaller binding energy it is conventional to use a reversed x-axis for the binding energy. The y-axis gives the number of electrons measured for a certain kinetic energy. The spectrum covers an energy interval from 57 eV to 67 eV including the Ir $4f_{5/2}$ and Ir $4f_{7/2}$ peaks. One can observe an increasing background at the high binding energy side, which occurs due to inelastic scattered electrons.
In order to work with such a spectrum several things have to be done. First of all one has to mention that the x-axis does not contain absolute binding energies of the core

electrons. However, we can calibrate the binding energy scale with the help of panel (b) as the absolute binding energy is by definition the position of the core peak relative to the fermi level of the sample. The fermi level of the sample can be obtained by measuring the binding energy interval of -1 to 1 eV of the sample i.e. one measures the electrons with a kinetic energy similar to the photon energy. The fermi level is then used to calibrate the spectrum properly. The next two steps are removing the background, which is often achieved by removing a polynomial fit which is weighted to the background regions, and calibrating the intensity of the spectrum. There are several options to calibrate the intensity. First, one can calibrate it to a peak height and set its intensity to 1. A second options is to calibrate to the area and a third option is to calibrate to the background, by dividing by the background counts on the lower binding energy side.

3.3.2 Core level shifts

The chemical environment of a core level electron determines its binding energy. Hence, a core electron of a free atom has a different binding energy than one of the same atom bound in a solid. The difference in energy between two atoms of the same kind is called core level shift (CLS). An example for CLS is shown in figure 8 (a). The spectrum shows the core levels of Ir $4f_{5/2}$ (first peak) and Ir $4f_{7/2}$ (second peak) electrons. For each peak one observes two peaks. The two components for each peak occurs due to a core level shift of the surface atoms. Their chemical environment is different as a result of the missing iridium atoms on top of the surface atoms. This results in an energy shift to, in this case, lower binding energies. The relative size of the surface component can be used to estimate the probing depth of the experiment. With a ratio of $\sim$ 1:1 between the surface and bulk components, it is obvious to conclude that we probe $\sim$ two atomic layers. The same element bound to a different element will have a characteristic CLS, which makes it possible to get information about the surface structure of the sample.

3.4 Data analysis

Data analysis is performed with the computer program IGOR PRO. Every component consists of different parameters. The width of the component is a result of the lifetime (Δ) t of the core hole. It can be determined by Heisenbergs uncertainty principle $\Delta E \cdot \Delta t \geq \frac{\hbar}{2}$ which would give every component a Lorentzian shape. In addition to the Lorentzian broadening each component is broadend by the resolution of the detector and the incoming photon. These uncertainties will result in a Gaussian broadening. A correct fit for the component contains therefore a convolution of a Lorentz function,

$$f(x; x_0, \gamma) = \frac{1}{\pi\gamma} \frac{\gamma^2}{(x - x_0)^2 + \gamma^2} \tag{8}$$

and a Gaussian function,

$$f(x) = a \exp - \frac{(x-b)^2}{2c^2} \tag{9}$$

which often is called a Voigt function:

$$V = G * L = \int_{\infty}^{-\infty} g(x) \cdot f(x - x') \mathrm{d}x' \tag{10}$$

Since the Voigt function takes a lot of time and computer power to perform, I will use an approximation for my analysis. Another problem arises due to inelastic scattering of the electrons. Electrons can only lose energy prior to reaching the detector by inelastic scattering with other atoms. The energy loss gives every component an asymmetric shape towards higher binding energies. Taking this into account modifies the Voigt function.
In total there are the following parameters: intensity of the peak, Gaussian width, Lorentzian width, binding energy and asymmetric behavior. Taking the ratio of two different components can give a quantitative estimate of the concentration of the atomic bindings. However, it is not possible to calculate absolute values, since many factors like X-ray flux, cross section of scattering or beam area are not properly determined.

3.5 Experimental details

The XPS measurements were performed at the spectroscopy endstation at beamline I311 of the MAX II storage ring at the MAX IV laboratory. The setup consists of a preparation and an analysis chamber with a base pressure of $5 \cdot 10^{-10}$ mbar. A Ir(111) sample was used as the substrate for the graphene growth. Ir(111) was cleaned by argon sputtering (1 kV) at room temperature followed by an oxygen treatment at 1120 K for 5 minutes. The cleanliness was checked by several XPS spectra. Afterwards one monolayer of graphene was grown in alignment with the previously presented procedures of TPG, 30 s of C_2H_4 at room temperature and a pressure of $1 \cdot 10^{-7}$mbar, followed by flashing to 1300 K and CVD for 30 minutes at 1170 K at the same pressure.
The second step of the experiment was exposing the graphene film to oxygen radicals for 270 s. This was achieved by an oxygen cracker, which was operated at a temperature of 1330°C. In order to avoid beam damage the following XPS measurements were recorded in a scanning mode with a scanning speed of 0.005 mm/s. The final step of the experiment was to expose the oxygen exposed sample to cobalt in an oxygen pressure of $1 \cdot 10^{-5}$mbar. The cobalt source was operated at a flux of 50 nA for 10 sec, which corresponds to a coverage of 0.16 ML.
The supporting STM measurements were performed in the STM lab Obelix of Lund university. Its setup consists also of a preparation and an analysis chamber with a base pressure of $7 \cdot 10^{-10}$ mbar and $5 \cdot 10^{-11}$ mbar respectively. The cleaning procedure of the Ir(111) was similar, however, we used 0.5 ML graphene grown by 3 cycles of TPG instead of one monolayer. Cleanliness of the iridium sample and the 0.5ML graphene were verified by LEED and STM.

4 Results and discussion

The results part is focused predominantly on the data recorded in the XPS measurements. I will analyze the C 1s, Ir $4f_{7/2}$, O 1s, and Co 2p spectra of each preparation step beginning with the Gr/Ir(111) preparation. The second sets of spectra are recorded after exposing the Gr/Ir(111) to atomic oxygen and the last sets after subsequent deposition of cobalt oxide.

4.1 Clean graphene

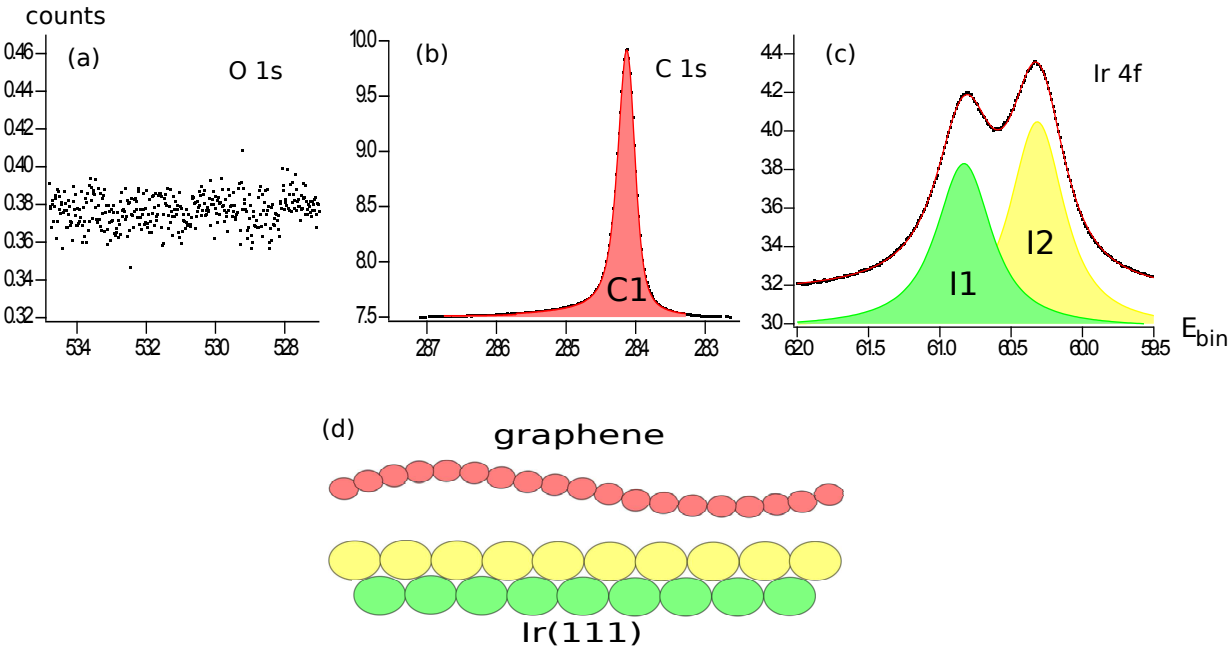

Figure 9: Panel (a), (b) and (c) show the O 1s, C 1s and Ir 4f spectra of clean graphene on Ir(111). The spectra are ordered according to their binding energies on the x-axis. The y-axis is proportional to the observed counts. Panel (d) shows an atomic model sketch of the current state of the experiment.

Figure 9 shows three different XPS spectra of a pristine graphene film and an atomic model sketch of the experiment. I will discuss these three spectra, starting with the Ir $4f_{7/2}$ followed by the O 1s and C 1s.

4.1.1 Ir $4f_{7/2}$

Panel (c) of figure 9 shows the Ir $4f_{7/2}$ spectra of clean graphene. A photon energy of 120 eV was used to record the data. A polynomial background was subtracted from the raw data. The intensity is normalized to the bulk peak. It displays two overlapping

peaks; the bulk peak at 60.83 eV (I1) and the surface peak at 60.31 eV (I2).

4.1.2 O 1s

The oxygen spectrum acquired after the growth of one mono layer graphene is presented in panel (a). The spectrum was recorded with a photon energy of 625 eV and is normalized to its background, which was subsequently removed by a polynomial fit. The spectrum shows a noisy flat line, which implies that oxygen is absent in the graphene film.

4.1.3 C 1s

The C 1s spectrum of the pristine graphene film is shown in panel (b). It was recorded with a photon energy of 390 eV. A polynomial background was removed and the intensity was normalized by setting the integral of the C 1s peak equal to one. For a clean monolayer of graphene a single slightly asymmetric peak with a binding energy of 284.13 eV is observed.

4.2 Oxygen - graphene

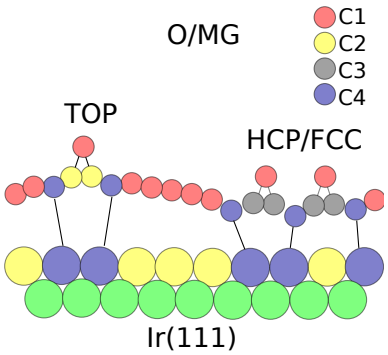

Figure 10: Two dimensional model sketch of the oxygen radical deposition onto graphene.

The second step of my experiment was the deposition of oxygen radicals onto the graphene. A model is shown in figure 10. Oxygen adsorption onto graphene/Ir(111) was studied recently by Vinogradov *et al.*[28]. The model in 10 is made according to their studies.
The carbon atoms bind to the oxygen radicals and form an epoxy group C-O-C with graphene, which thereof changes the carbons sp^2 hybridization to a sp^3 diamond like structure [28]. The new formed epoxy groups are responsible for a CLS in the C 1s spectrum. The binding energy for epoxy groups formed in the TOP domains is 285.9

eV and 285.6 eV in the HCP/FCC domains.
Both of the carbon atoms in an epoxy group are attracted towards the oxygen which raises them up, meanwhile their neighbour atoms are pulled downward closer to the Ir(111), which has the consequence of an orbital mixing between the carbon π orbitals and the 5d states of iridium [28]. The orbital mixing results in another CLS of +0.59 eV in the C 1s spectrum. That gives in total four components in the C 1s spectrum, respectively called C1, C2, C3 and C4 and one additional component in the Ir 4f spectrum. Even though, it is possible to differentiate between the HCP and FCC domains in the C 1s spectrum, Vinogradov *et al.* observed only one new component in the Ir 4f spectrum.

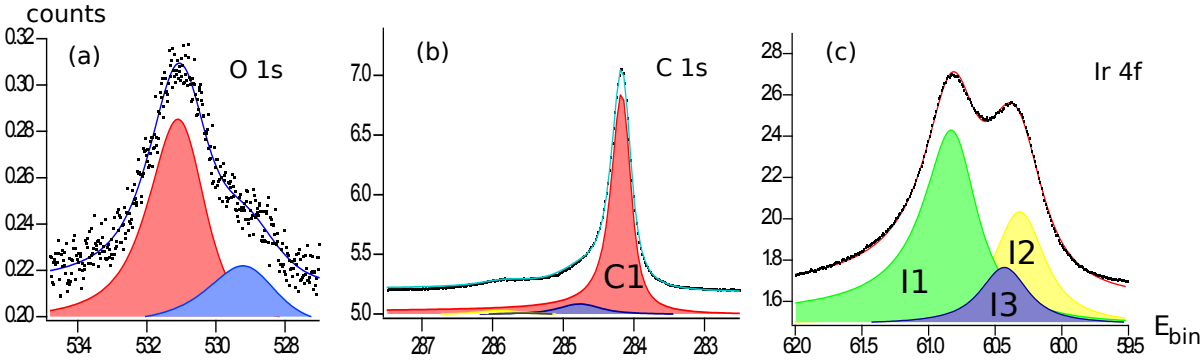

Figure 11: Panel (a), (b) and (c) show the O 1s, C 1s and Ir 4f spectra of oxygen modified graphene on Ir(111). The spectra are ordered according to their binding energies on the x-axis. The y-axis is proportional to the observed counts.

In figure 11 are three different XPS spectra after the deposition of oxygen atoms onto the graphene. The three spectra were recorded with the previously mentioned photon energies and their intensities and background were also modified accordingly.

4.2.1 Ir $4f_{7/2}$

The Ir $4f_{7/2}$ spectrum after dosing oxygen radicals is shown in panel (c) of figure 11. A comparison to the spectrum in figure 9 shows that the intensity of the Ir $4f_{7/2}$ surface peak becomes heavily reduced. For pristine graphene it was 20% higher than the bulk and now it is 20% lower than the bulk peak. The reduction correlates with the orbital mixing between carbon atoms and Ir(111) atoms. As introduced before carbon atoms of graphene bind downward to the Ir(111) substrate atoms. Hence, there is a third, blue, component (I3) in the Ir $4f_{7/2}$ spectrum with a binding energy of 60.43 eV. Vinogradov *et al.* found in their study a binding energy of 60.75 eV for this component, which is a difference of +0.22 eV to the value I observed. This difference could occur as consequence of the lower oxygen dose I used. However, this is of no importance for the outcome of this thesis and it will not be discussed further. With the intensities of the components

I2 and I3 it is possible to determine the oxygen coverage. The integral values of 0.312 and 0.133, respectively, result in $\approx 30\%$ of the Ir(111) atoms bound to the graphene. A moiré cell with in average 87 iridium atoms has therefore 26 iridium atoms that are bound to the graphene. Considering the 2:1 ratio between the C4 component and the epoxy group, this leads to 13 carbon atoms out of 200, that are bound to the oxygen, which is equivalent to a coverage of 6.5%.

4.2.2 O 1s

Panel (a) shows the O 1s spectrum after dosing oxygen radicals for 270s. Now one peak is observed at a binding energy of 531.1 eV with a shoulder towards lower binding energies. The main peak is assigned to the epoxy group ($C-O-C$), while the second component is not correctly assigned yet. Vinogradov *et al.* suggest that it could belong to intercalated oxygen [28]. Intercalated oxygen was studied later by Grånäs *et al.*, who found a binding energy of 529.9 eV [29]. Curve fitting reveals a binding energy of 529.2 eV for the second component incompatible with oxygen intercalation. Furthermore there are no signs of intercalation in the Ir 4f spectrum, which should give rise to additional new components.

4.2.3 C 1s

After exposing the graphene to atomic oxygen for 270s one observes a single asymmetric peak again, panel (b), at a binding energy of 284.18 eV (C1). However, this time the peak has a shoulder to the higher binding energy side. In addition to this, the peak is more broadened. A four component plot, in accordance with Vinogradov *et al.*, provides binding energies of 284.18 eV for the main peak (C1), 285.9 for C2, 285.6 eV for C3, and 284.77 eV for the fourth component (C4). These binding energies are consistent with the data of Vinogradov *et al.*[28]. Figure 12 shows a zoom-in to the shoulder of the C 1s spectrum of after deposition of oxygen radicals onto the graphene.

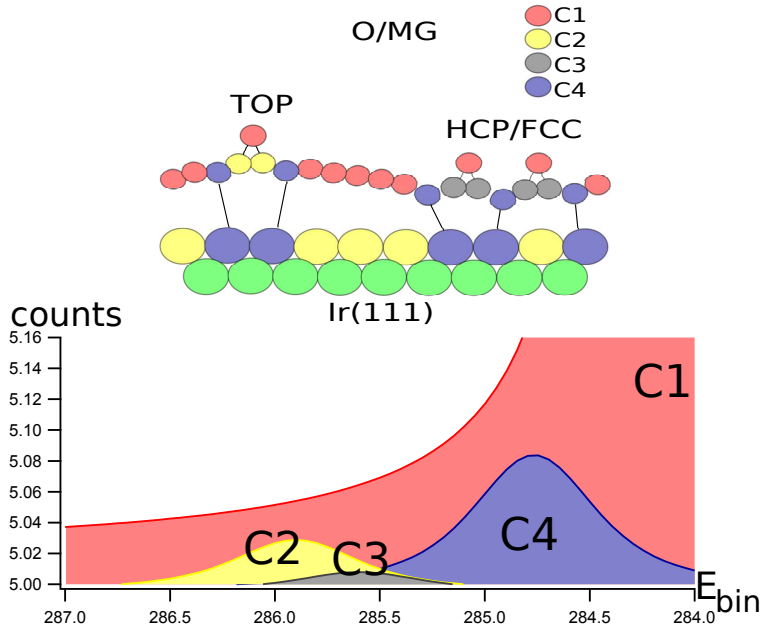

Figure 12: A zoom-in to the shoulder of the C 1s spectrum after deposition of oxygen radicals onto the graphene.

Several restrictions were used for the curve fitting of the C 1s spectrum in figure 12 and panel (b) of figure 11. To decrease the degrees of freedom the components C2, C3 and C4 share the same Lorentzian and Gaussian width parameter. As seen from the curve fitting the amplitudes, and thereby the intensities, of the components C2, C3 and C4 are quite different, with C4 having the highest intensity. The intensities of C2 and C3, especially, are so small compared to the asymmetric tail of the C1 component that it is difficult to make reliable physical predictions from them. Hence, they have very large error bars. Vinogradov *et al.* found in their study for low oxygen doses, which is the case for this experiment, a larger C3 component indicating a higher coverage in the HCP and FCC domains. Their observation is explained by the carbon π orbitals that can interact more easily with the iridium in the HCP/FCC domains as they are closer to the metal, which makes it more likely for the oxygen to bind there. [28]
The intensity of the C4 component should according to the theory for low coverages be twice as much as the sum of the intensities of C2 and C3 (I(C4)=2(I(C2)+I(C3))), since every carbon atom in epoxy group has two additional neighbor atoms. This results in 4 atoms with a C4 characteristic for every epoxy group; hence, the 1:2 ratio. Furthermore one is able to calculate the oxygen coverage with the intensity of C4. I normalized the spectrum to an area of 1 below the peak. The oxygen coverage corresponds to the intensity of C4 divided by 2, i.e. the number of carbon atoms bound in an epoxy group. The intensity of the C4 component is 0.065, which means that $\approx$ 3.3% of all carbon atoms are bound in an epoxy group. A similar calculation with the values obtained by the Ir 4f spectrum provided a coverage of 6.5%, which is twice as high. Due to the large uncertainty in the C 1s curve fitting the value of the Ir $4f_{7/2}$ is more likely to represent the real coverage of the graphene.

4.3 Cobalt oxide - oxygen - graphene

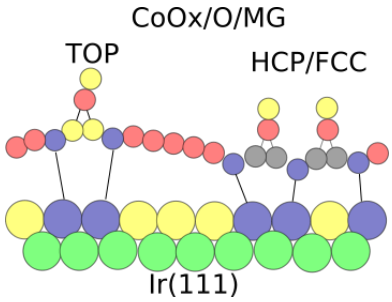

Figure 13: Two dimensional model sketch of cobalt oxide deposition onto oxygen modified graphene.

The third and last step of my experiment was the deposition of cobalt oxide onto the sample. This is shown in the model sketch of figure 10. It shows cobalt oxide molecules (in yellow) sitting on top of the epoxy groups, but not on the graphene.

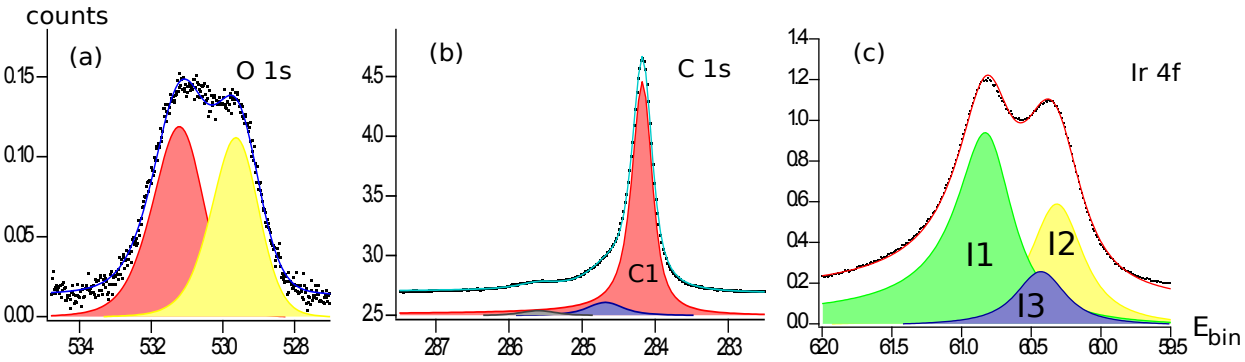

Figure 14: Panel (a), (b) and (c) show the O 1s, C 1s and Ir 4f spectra after deposition of cobalt oxide on O-functionalized graphene. The spectra are ordered according to their binding energies on the x-axis. The y-axis is proportional to the observed counts.

Figure 14 shows three different XPS spectra after the deposition of cobalt oxide molecules onto the sample. The three spectra were recorded with the previously mentioned photon energies and their intensities and background were also modified accordingly.

4.3.1 Ir $4f_{7/2}$

The deposition of cobalt oxide does not change the Ir $4f_{7/2}$ spectrum much as seen by comparison of between the panels (c) of figures 11 and 14. All three components

have almost equal intensities. There seems to be no intercalation of cobalt or oxygen between Gr and Ir(111), since we do not observe any new components in the Ir 4f region. In summary, the deposition of cobalt oxide has no influence on the Ir 4f core levels and I thereof conclude that the Ir-Gr binding is unchanged upon cobalt oxide deposition.

4.3.2 O 1s

In contrast to the Ir 4f spectrum the O 1s spectrum changes significantly. Now a broad peak, which appears to be a superposition of two components, is observed. A two component fit reveals a binding energy for the epoxy group of 531.2 eV, which is a shift of +0.1 eV compared to panel (b), and for the cobalt oxide component of 529.6 eV. The reason for the shift of the epoxy groups binding energy is probably the binding of cobalt oxide to the epoxy groups. The intensity of the two peaks differs by less than 10 %. Hence, there is almost as much oxygen bound to the cobalt as oxygen radicals on the graphene.

4.3.3 C 1s

The C 1s spectrum shows again a single asymmetric peak with a shoulder to the higher binding energy side. A zoom-in, like in figure 15, to the shoulder of the C 1s spectrum reveals that its shape changed slightly.

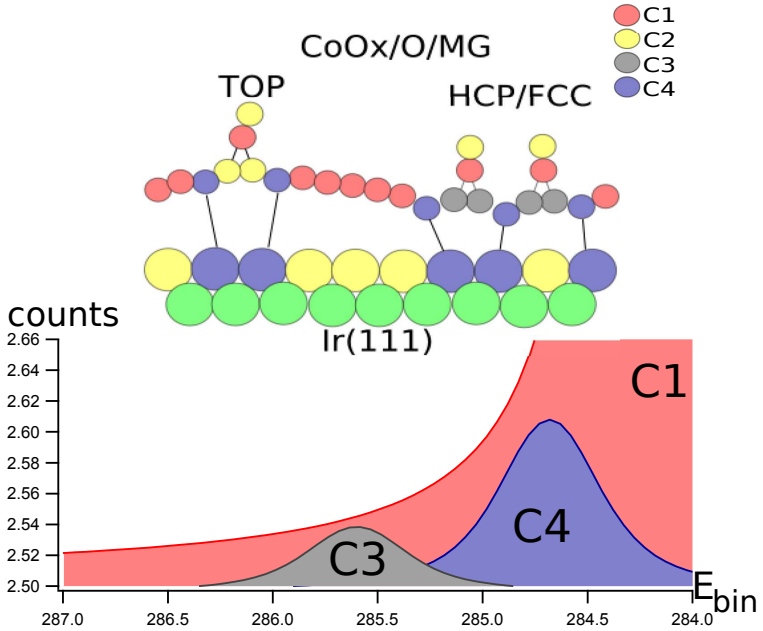

Figure 15: Zoom-in to the shoulder of the C 1s spectrum after deposition of oxygen radicals onto the graphene.

The curve fitting provides new intensities for the components C2, C3 and C4. The amplitude of the C1 component and main peak is higher than in the previous spectrum, but the intensity for this component does not change; the change in amplitude is connected to a small change in Lorentzian and Gaussian width in the plot. The intensity of the C2 component almost disappears, while the intensity of the C3 increases. The intensity of the C3 component is, however, still very small compared to the tale of the C1 component. Nevertheless, its intensity of 0.023 suggests a total coverage of 2.3%; i.e. 2.3% of all carbon atoms are bound to oxygen radicals. Furthermore, since the C3 component corresponds to oxygen in the HCP and FCC domains, the data are now in line with the observations of [28]. The ratio between C3 and C4 should according to the theory be 1:2 but with the values provided by the plot it is 1:3. In addition to this incorrect ratio, the C4 peak is shifted slightly in energy to 284.68 eV, a shift of (+0.50 eV) compared to the main peak. The combination of these two facts lead to the conclusion that there could be a new component close to C4. The change in intensity, especially, of the C2 and C3 components is not necessarily a result of a change in the experiment, but could be a result of the large error bars of these components.

4.3.4 Co 2p

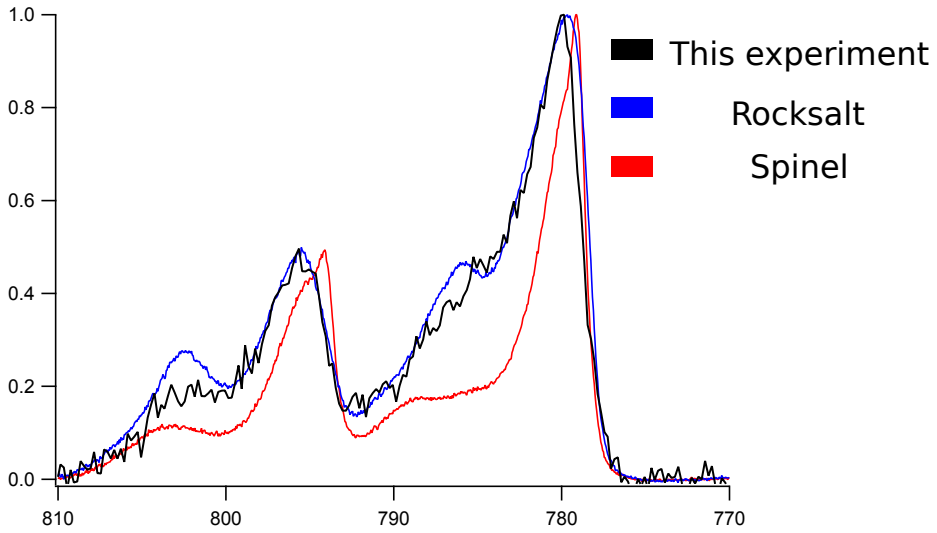

Figure 16: Black spectrum: Co 2p spectrum after deposing cobalt for 10s in an oxygen pressuret of 10^{-5}mbar onto O-functionalized Gr/Ir(111). Red spectrum is of a spinel film (Co_3O_4), while the blue spectrum represents rocksalt structure (CoO).[30]

Additionally to the three previously discussed spectra, I recorded the Co 2p spectrum after the deposition of cobalt oxide onto the sample. Figure 16 shows three different Co 2p spectra each plotted with different color. The black spectrum was recorded with a photon energy of 1100 eV after deposing cobalt oxide onto the O-functionalized graphene

sample. All three spectra are normalized to their highest peak point after removal of a polynomial background. The blue and red spectra are reference spectra of rocksalt CoO(111) (blue) and spinel Co_3O_4 (red) films recorded in a previous experiment [30]. Each spectrum shows two main peaks (Co $2p_{3/2}$ and Co $2p_{1/2}$) with shoulders at the high binding energy side. The binding energies of the same cobalt peaks, but for the spinel and the rocksalt structure, differ in more than 1 eV and the shoulders are clearly more pronounced for the rocksalt (CoO(111)) structure. Both the peak position and the shape of the blue and black spectra are quite similar suggesting that my cobalt oxide particles are rocksalt like.

5 Conclusion

Summarizing my results, I successfully deposed and characterized oxygen radicals on graphene. The oxygen radicals lead to an epoxy group (C-O-C) that prefers to sit in the HCP/FCC domains. The Ir $4f_{7/2}$ spectrum suggests that 6.5% of all carbon atoms are bound in an epoxy group. This value seems more reasonable than the ones of the C1s spectrum due to high uncertainties as a consequence of the low coverage. Deposition of cobalt oxide onto the O-functionalized graphene led to a rocksalt structure, which is confirmed by comparing the Co 2p spectrum to reference spectra. Intercalation of cobalt or oxygen could be excluded based on the Ir 4f spectra, that shows no new components. The small energy shift for the epoxy group in the O 1s spectrum and its 1:1 ratio to the cobalt oxide component suggest that the cobalt oxide is located on top of the O-functionalized graphene film and forms clusters. However, a direct cobalt oxide - graphene binding can not be excluded with safety, though the high dosage of cobalt oxide should then lead to a new visible component in the C 1s spectrum. Further XPS experiments with a higher oxygen dosage and STM measurements have to be performed in order to make reliable predictions.

6 Outlook

Previously discussed results suggest that there is cobalt oxide sitting in a rocksalt structure on top of the epoxy groups of the graphene. Further STM experiments after cobalt oxide deposition onto O-functionalized graphene are needed to confirm or reject that I have successfully grown well-ordered cobalt oxide clusters. The figures 17 and 18 show STM images of a similar experiment with 0.5 ML Gr/Ir(111).

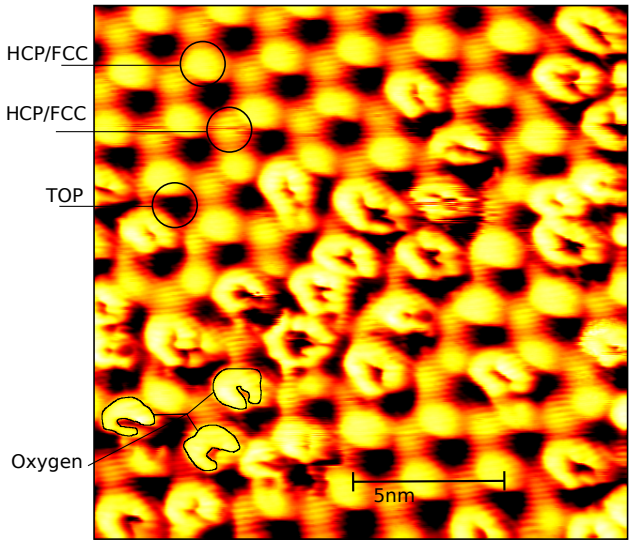

Figure 17: 17 nm x 17 nm STM image of atomic oxygen on top of 0.5Ml GR/Ir(111) with visible moiré pattern. Bright spots on top of the moiré pattern correspond to the epoxy groups, Parameters: 100 pA, 1.50 V.

A STM image, acquired after dosing oxygen radicals for 4 minutes onto 0.5 ML graphene, is shown in figure 17. In the picture the moiré pattern of graphene on Ir(111) is clearly visible. The bright regions in yellow/orange are the HCP and FCC domains, while the black regions are the TOP domains. In contrast to the STM images of pristine graphene shown in figure 7 one can this time differentiate between HCP and FCC domains, although it is not possible to say which of the two bright domains presents HCP or FCC domains. Within the image unordered additional components (bright spots) are observed in some of the domains. Inspection of the image reveals that these bright spots are located in the HCP and FCC domains. Since no such bright spots were observed before the dosing of oxygen radicals, I conclude that the bright spots in the HCP/FCC domains are due to epoxy groups found in these domains. This observation is in line with previous performed experiments. [28]

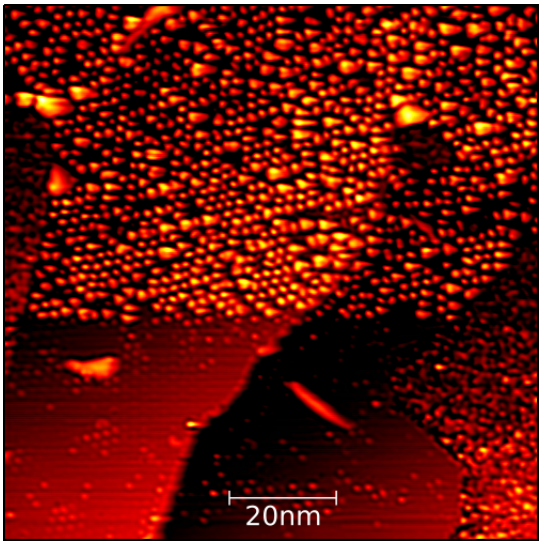

Figure 18: STM image of cobalt oxide on 0.5MG/Ir(111). The image was recorded with a current of 60pA and a bias of 2.70V.

Another STM image, recorded after the deposition of cobalt oxide on 0.5ML Gr/Ir(111) is presented in figure 18, experiment condition and dosage are similar to the previous discussed data. The bright spots in the pictures refer to cobalt oxide. They seem to be arranged in clusters, which supports the results obtained by the C 1s spectrum. Nonetheless, one can not exclude intercalation of cobalt beneath the graphene due to the use of 0.5MG. Intercalation would also explain the border between graphene with lots of cobalt oxide and with less amount of bright spots. Furthermore the image gives no indication whether the cobalt oxide sits in the TOP, in the HCP/FCC domains on oxygen or directly on the graphene. To avoid intercalation new STM experiments of cobalt oxide deposition onto O-functionalized 1 ML graphene are planned.

Acknowledgements

Last but not least, I want to acknowledge the help and support I got from several people during the last 4 months writing this thesis.
First, I want to thank my supervisor Jan Knudsen for giving me the opportunity to work in a real research project as part of my Bachelor thesis. Furthermore, for all the feedback and teaching I got, especially when it came to actually put the results into words.
I also want to thank Md. Alif Arman, for the company in the STM lab or during the night shifts while acquiring the XPS results. Moreover, for all the introductions and answered questions regarding experimental setups and details.
During the two weeks of XPS measurements, I enjoyed the company and help of the research group around Thomas Michely. Therefore I want to thank him and additionally, Ulrike Schröder, Charlotte Herbig and Antonio Martinez-Galera.
Finally, I want to thank Melissa Harris for proof reading and helping me with the language.

References

[1] Bockris JO, Dandapani B, Cocke D, Ghoroghchian J. On the splitting of water. International Journal of Hydrogen Energy. 1985;10 (3):179–201.

[2] LaMonica M. A Cheaper Way to Make Hydrogen from Water. MIT Technology review. 2013 March;Www.technologyreview.com/view/512996/a-cheaper-way-to-make-hydrogen-from-water/.

[3] Jiao F, Frei H. Nanostructured Cobalt Oxide Clusters in Mesoporous Silica as Efficient Oxygen-Evolving Catalysts. Angew Chem Int Ed. 2009;48.

[4] Novoselov KS, Geim AK, Morozov S, Jiang D, Zhang Y, Dubonos S, et al. Electric field effect in atomically thin carbon films. science. 2004;306(5696):666–669.

[5] Posternak M, Baldereschi A, Freeman A, Wimmer E. Prediction of electronic surface states in layered materials: graphite. Physical review letters. 1984;52(10):863.

[6] Geim AK, Novoselov KS. The rise of graphene. Nature materials. 2007;6(3):183–191.

[7] Nordling C, Osterman J. Physics Handbook for Science and Engineering, 6th ed. Studentlitteratur, Lund; 2002.

[8] Lee C, Wei X, Kysar JW, Hone J. Measurement of the elastic properties and intrinsic strength of monolayer graphene. science. 2008;321(5887):385–388.

[9] Liu F, Ming P, Li J. Ab initio calculation of ideal strength and phonon instability of graphene under tension. Physical Review B. 2007;76(6):064120.

[10] COMMISSION E, editor. FET Flagships: A novel partnering approach to address grand scientific challenges and to boost innovation in Europe. vol. 283 final; 2014.

[11] Coraux J, Plasa TN, Busse C, Michely T, et al. Structure of epitaxial graphene on Ir (111). New Journal of Physics. 2008;10(4):043033.

[12] Grånäs E. Above and Below Graphene: Nanoparticle Chemistry and Interface Reactions. Lund University; 2014.

[13] Cooper DR, D'Anjou B, Ghattamaneni N, Harack B, Hilke M, Horth A, et al. Experimental review of graphene. International Scholarly Research Notices. 2012;2012.

[14] Ohta T, Bostwick A, Seyller T, Horn K, Rotenberg E. Controlling the electronic structure of bilayer graphene. Science. 2006;313(5789):951–954.

[15] Bleikamp S, Feibelman PJ, Michely T, et al. Two-dimensional Ir cluster lattice on a graphene moiré on Ir (111). Physical Review Letters. 2006;97(21):215501.

[16] Feibelman PJ. Pinning of graphene to Ir (111) by flat Ir dots. Physical Review B. 2008;77(16):165419.

[17] Coraux J, N'Diaye AT, Busse C, Michely T. Structural coherency of graphene on Ir (111). Nano letters. 2008;8(2):565–570.

[18] Lizzit S, Baraldi A. High-resolution fast X-ray photoelectron spectroscopy study of ethylene interaction with Ir (111): From chemisorption to dissociation and graphene formation. Catalysis Today. 2010;154(1):68–74.

[19] Kralj M, Pletikosić I, Petrović M, Pervan P, Milun M, Busse C, et al. Graphene on Ir (111) characterized by angle-resolved photoemission. Physical Review B. 2011;84(7):075427.

[20] Coraux J, Engler M, Busse C, Wall D, Buckanie N, Zu Heringdorf FJM, et al. Growth of graphene on Ir (111). New Journal of Physics. 2009;11(2):023006.

[21] Van Gastel R, N'Diaye A, Wall D, Coraux J, Busse C, Buckanie N, et al. Selecting a single orientation for millimeter sized graphene sheets. Applied Physics Letters. 2009;95(12):121901.

[22] Binnig G, Rohrer H. Scanning tunneling microscopy. IBM Journal of research and development. 2000;44(1-2):279–293.

[23] of Sciences RSA. Press release of The Royal Swedish Academy of Sciences; 1986. 15 October.

[24] Attard G, Barnes C. Surfaces, Oxford Chemistry Primers, 1 ed. New York: Oxford University Press; 2009.

[25] Einstein A. Über einen die Erzeugung und Verwandlung des Lichtes betreffenden heuristischen Gesichtspunkt. Annalen der Physik. 1905;322(6):132–148.

[26] Hertz H. Ueber einen Einfluss des ultravioletten Lichtes auf die electrische Entladung. Annalen der Physik. 1887;267(8):983–1000.

[27] org N. The Nobel Prize in Physics 1921; 1921. Available from: `www.webcitation.org/5bLXMl1V0`.

[28] Vinogradov N, Schulte K, Ng ML, Mikkelsen A, Lundgren E, Mårtensson N, et al. Impact of atomic oxygen on the structure of graphene formed on Ir (111) and Pt (111). The Journal of Physical Chemistry C. 2011;115(19):9568–9577.

[29] Gråsäs E, Knudsen J, Schröder UA, Gerber T, Busse C, Arman MA, et al. Oxygen intercalation under graphene on Ir (111): Energetics, kinetics, and the role of graphene edges. ACS nano. 2012;6(11):9951–9963.

[30] Knudsen J, Arman MA, et al.. Cobaltoxide; 2015. Lund University.